Path Planning Technology for Unmanned Aerial Vehicle Swarm Based on Improved Jump Point Algorithm

Haizhou Zhang*, Shengnan Xu
School of Information Engineering, Henan Vocational University of Science and Technology, Zhoukou, Henan, 466000, China

***Abstract*—Multi-unmanned aerial vehicle path planning encounters challenges with effective obstacle avoidance and collaborative operation. The study proposes a swarm planning technique for unmanned aerial vehicles, based on an improved jump point algorithm. It introduces a geometric collision detection strategy to optimize path search and employs the dynamic window method to constrain the flight range. Additionally, the study presents conflict avoidance strategies for multi-unmanned aerial vehicle path planning and establishes collision fields for unmanned aerial vehicles to achieve collaborative path planning. In single unmanned aerial vehicle path planning, the research model exhibits the lowest control errors in the X, Y, and Z axes, with the Y-axis error being 0.05m. In static planning, the model boasts the shortest planning time and length, with 1002ms and 17.85m in multi-obstacle planning, respectively. In multi-unmanned aerial vehicle path planning, the research model effectively avoids local optimal problems in local conflict scenarios and re-plans the route. During testing on a 29m×29m grid map, the research technology successfully avoids obstacles and re-plans routes. However, similar technological obstacles can cause interference and traps in local convergence, preventing re-planning. The research technology demonstrates good application effects in the path planning of unmanned aerial vehicle swarms and will provide technical support for multi-machine collaborative path planning.**

Keywords*—Unmanned aerial vehicle swarm; path planning; jump point search algorithm; geometric collision detection; dynamic window method

I. INTRODUCTION

With the development of unmanned aerial vehicle (UAV) technology, the potential application of multi-UAV cooperative planning in military reconnaissance, environmental monitoring, disaster rescue, and other fields is enormous. However, the planning for multiple UAVs is constrained by the control of these UAVs and the impact of obstacles, leading to poor coordination among the UAVs and challenges in meeting flight requirements. Therefore, scholars have conducted extensive research on collision planning techniques for UAV swarms to improve the effectiveness of UAV swarm planning [1]. Shen K et al. studied the problem of insufficient path planning (PP) for multi-warehouse UAVs and proposed a PP method that considers collision avoidance. This method optimized the route by establishing a multi-warehouse UAV PP model, taking into account factors such as UAV flight distance, time, and cargo loading capacity. Flight tests showed that this method could reduce UAV costs and improve technical planning efficiency [2]. Meng S et al. conducted research in the field of UAV detection. To improve the coordination effect of multiple UAVs, image denoising technology was introduced to optimize feature extraction and enhance the processing and analysis of object edge details. Tests showed that this technology could substantially raise the obstacle avoidance ability and crack object detection performance of UAVs [3]. Bui S T et al. conducted research on the insufficient adaptability of UAVs for takeoff, landing, and collision, and proposed a biomimetic propeller design for UAVs. This design was inspired by the flexibility and elasticity of dragonfly wings, which can adapt to collisions and quickly recover and hover. Tests showed that the proposed propeller had good adaptability and could effectively optimize the collision effect of UAVs [4]. Fahimi H et al. proposed a vision-based guidance algorithm to enhance the obstacle avoidance capability of UAVs. It was equipped with cameras inside the UAV, which detected object edge details through algorithms, optimized the captured image details using algorithms, and provided flight decisions for UAV obstacle avoidance. The results indicated that UAVs could effectively avoid obstacles in flight scenarios and improve the planning efficiency of UAVs [5].

At present, multi-UAV collaborative PP is a key focus of UAV development. Saeed R A et al. conducted research on PP for UAV swarms. To improve the obstacle avoidance and planning effectiveness of UAVs, a three-dimensional scene multi-UAV planning technology based on ant colony algorithm was proposed, and the technology was improved through conditional constraints and collision strategies. The results indicated that the technology had good planning performance [6]. Puente Castro A et al. studied the problem of insufficient PP for UAV swarms and proposed a solution based on artificial intelligence algorithms. The study conducted research on the latest UAV planning technologies, selected the latest technologies through classification and comparison, and summarized the limitations of current research. The results indicated that artificial intelligence planning scenarios were limited by computation and complex conditions, and had limited adaptability [7]. Dhuheir M A et al. proposed a distributed collaborative inference request and PP model to tackle the problem of insufficient reasoning in UAV PP. This model divided inference requests into multiple parts and executes them in different UAVs to reduce data transmission latency and interference. Experimental tests showed that this technology had good adaptability, but communication and collaboration still faced difficulties [8]. Sharma A et al. studied the PP problem for UAV swarm interception of multiple aerial

*Corresponding Author

targets and proposed a solution based on swarm intelligence algorithm. The team conducted a comprehensive analysis and improvement of swarm intelligence algorithms such as particle swarm optimization (PSO) and ant colony optimization. In practical scenario testing, different algorithms had limited adaptability in complex environments and diverse target interception tasks, and the impact of dynamic obstacle scenarios needed to be considered [9]. Yu Z et al. proposed a new hybrid PSO algorithm for automatic PP of UAVs. This algorithm improved the global optimal solution update strategy and particle learning strategy of PSO algorithm by integrating simulated annealing algorithm, enhancing optimization ability and convergence speed. Experimental tests showed that the proposed technology could adapt well to the 3D scene planning effect of UAVs [10].

In summary, multi-UAV planning is the key to the development of UAV technology. However, PP for multiple UAVs is more complex, and how to avoid obstacles and coordinate the fleet is a technical challenge. At present, technologies such as ant colony algorithm, particle algorithm, and bat algorithm have good advantages in PP, but they still face problems such as high computational cost and insufficient planning for complex dynamic scenes in multi-UAV scenarios. Therefore, in order to solve the problem of insufficient PP for UAV swarms, an intelligent UAV swarm PP technology based on an improved Jump Point Search (JPS) algorithm is proposed. There are two innovations in this technology. Firstly, the introduction of geometric collision detection strategy in the research improves the shortcomings of JPS node search. Meanwhile, Dynamic Window Approaches (DWA) are introduced for obstacle avoidance optimization to enhance the accuracy of PP. Secondly, the research focuses on adding conflict avoidance strategies in multi-UAV PP, setting avoidance specifications through the division of collision fields, and enhancing the obstacle avoidance capabilities of UAV swarms. The research has two contributions. One is that the technology provides technical support for single UAV PP and improves its ability of obstacle avoidance and dynamic planning in complex environments. The second is that the research provides technical support for the cooperative operation of multiple UAVs, and helps the UAV cluster to effectively coordinate and avoid conflicts in complex tasks.

II. Methods and Materials

A. Modeling of Single UAV PP Based on Improved JPS

The process of UAV PP needs to consider various threats and limitations in the environment to avoid collisions during flight. Therefore, the PP modeling of single UAV based on improved JPS algorithm is studied. Aiming at the environmental threat and collision risk in UAV PP, the improved JPS algorithm is introduced as the global planning technology, and combined with DWA algorithm to optimize the local planning. The JPS algorithm, which is based on a grid map, employs the JPS strategy to identify feasible nodes and optimizes the path using a geometric collision detection strategy. DWA algorithm can adjust the speed and direction of UAV in real time and improve the effect of dynamic planning by constructing speed space and dynamic window. The entire technical process is shown in Fig. 1.

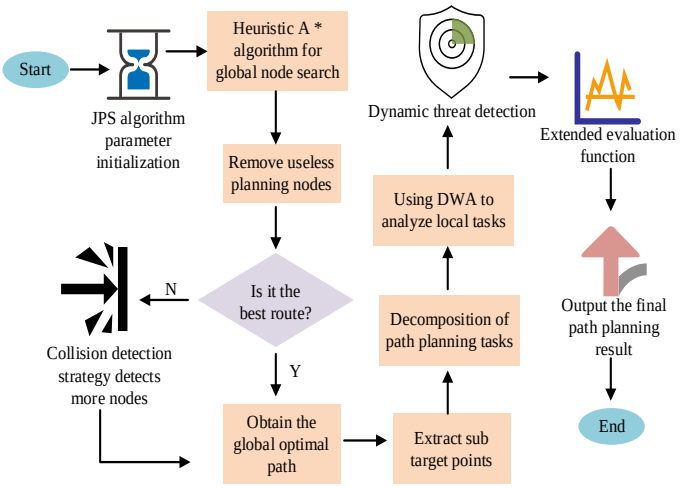

Fig. 1. Single UAV PP technology.

From Fig. 1, this technology uses the JPS algorithm as the global PP core, while adopting DWA as the local planning to improve the dynamic planning effect of UAVs. In the scope of UAV planning, JPS is used to obtain feasible nodes, based on a grid map, where each grid contains 8 adjacent nodes. The JPS algorithm needs to remove useless nodes based on the adjacent node pruning strategy in order to search for the best planned path [11]. The evaluation function $R(n)$ is shown in Eq. (1).

$$R(n)=g(n)+h(n) \tag{1}$$

In Eq. (1), $h(n)$ represents the cost incurred from node n to the target node. $g(k)$ represents the optimal actual path cost from the initial to the current node n. In actual UAV planning, the JPS algorithm is affected by the expansion direction of grid nodes, and its planning can only choose 8 speed directions, which will significantly limit its planning effectiveness [12]. In this regard, the study introduces geometric collision detection strategies to optimize its planned path, thereby providing more selectable paths for UAVs. Among them, if the optional path is defined as $\pi' = (n_1, n_7, n_8)$, n_i is the path node, and the original path is $\pi = \{n_1, n_2, \cdots, n_8\}$, then the collision detection strategy is expressed as Eq. (2) [13].

$$\kappa(n_i, n_j) = \begin{cases} (n_i, n_j) & 0, \\ (n_i, n_j) & 1, \end{cases} \quad \forall n_1, n_j \in N \tag{2}$$

In Eq. (2), $\kappa(\square)$ is the detection function, n_i and n_j both are nodes within the original path set N. The study employs a collision detection strategy to identify nodes in the original path where collisions occur, represented as 1, and those without collisions, represented as 0. The principle of collision detection strategy path optimization is shown in Fig. 2 [14].

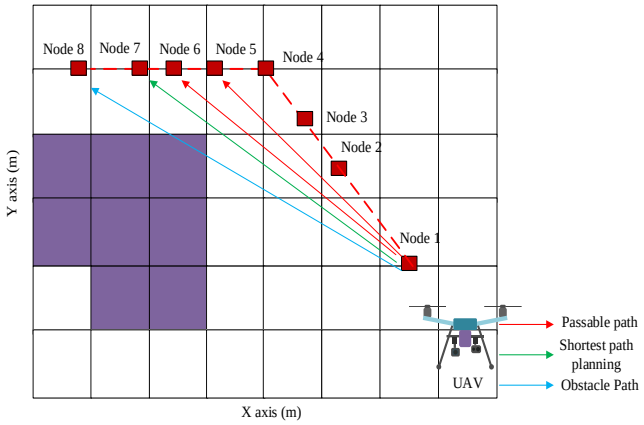

Fig. 2. Schematic diagram of collision detection strategy.

According to Fig. 2, in the original path search, this strategy identifies optional paths through geometric collisions to avoid obstacles. In addition, the study introduces the DWA algorithm as a local obstacle avoidance planning technique for UAVs, which has fast response and low computational complexity. In UAV collision control, it is necessary to construct a UAV motion model, as shown in Eq. (3).

$$\begin{cases} \xi(t_n) = \xi(t_0) + \omega(t)\Delta t \\ x(t_n) = x(t_0) + \int_{t_0}^{t_s} v(t)\cos\left[\theta(t)\right]dt \\ y(t_n) = y(t_0) + \int_{t_0}^{t_s} v(t)\sin\left[\theta(t)\right]dt \end{cases} \quad (3)$$

In Eq. (3), $\xi(t_n)$ represents the angle between the UAV and the X-axis at time t_n. ($x(t_n), y(t_n)$) is the coordinate of the UAV at time t_n. To satisfy the demands of UAV, it needs to satisfy motion model constraints, as shown in Eq. (4) [15].

$$\begin{cases} DS(x,y) \geq 0 \\ 0 \leq v \leq v_{\max} \\ \omega_{\min} \leq \omega \leq \omega_{\max} \\ \dot{v}_b \leq \dot{v}_{b\max} \end{cases} \quad (4)$$

In Eq. (4), $DS(x,y)$ represents the closest distance between the obstacle and the UAV. v indicates the linear velocity of the UAV. ω is the angular velocity of UAVs. $\dot{v}_b$ is the braking acceleration of the UAV's linear velocity. To ensure that the UAV maintains optimal planning performance within the constraint range, the DWA algorithm needs to construct a velocity space based on the UAV's own coordinates, as shown in Fig. 3 [16].

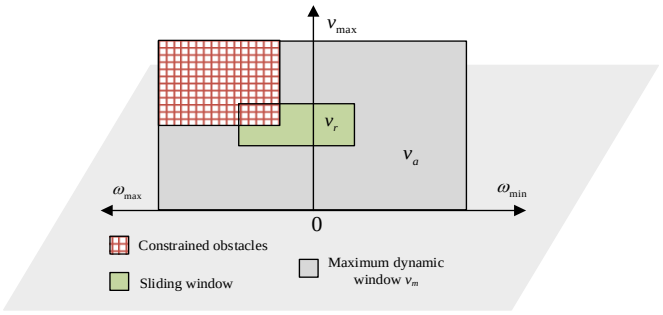

Fig. 3. UAV speed space.

In Fig. 3, a velocity space is established with the origin of the UAV as the coordinate, where the angular velocity is represented by the horizontal axis and the vertical axis is represented by the UAV linear velocity. When a UAV performs a flight mission, any cycle command is represented by (v, ω) and the UAV velocity space is composed of multiple (v, ω). The dynamic window is the speed range that the UAV can reach in the speed space [17]. The maximum dynamic window of the UAV is defined as V_m, expressed as Eq. (5).

$$V_m = \{(v,\omega) | 0 \leq v \leq v_{\max}, \omega_{\min} \leq \omega \leq \omega_{\max}\} \quad (5)$$

In an effective planning process, the UAV's speed is limited to prevent collisions with objects; upon a collision, the speed will drop to zero. The maximum dynamic window of the aircraft within the safe range is set as V_{safe}, as shown in Eq. (6) [18].

$$V_{safe} = \left\{(v,\omega) | v \leq \sqrt{2DS(v,\omega)\dot{v}_{b\max}}, \omega \leq \sqrt{2DS(v,\omega)\dot{\omega}_{b\max}}\right\} \quad (6)$$

In Eq. (6), $DS(v,\omega)$ is the distance between the UAV and the obstacle. $\dot{\omega}_{b\max}$ represents the maximum angular velocity braking acceleration of the UAV. Besides, the maximum speed of the UAV planning is influenced by its own acceleration capabilities, which further narrows the range of the maximum dynamic window V_m, particularly during obstacle avoidance when the speed is kept at a low level. [19]. Therefore, based on this, the dynamic window V_F is obtained as shown in Eq. (7).

$$V_F = \{(v,\omega) | v_c - \dot{v}_{b\max}\Delta t \leq v \leq v_c + \dot{v}_{a\max}\Delta t, \omega_c - \dot{\omega}_{b\max}\Delta t \leq \omega \leq \omega_c + \dot{\omega}_{a\max}\Delta t\} \quad (7)$$

In Eq. (7), ω_c represents the current angular velocity of the UAV, $\dot{\omega}_a$ is the maximum angular acceleration of the UAV, v_c is the current line velocity of the UAV, and $\dot{v}_{a\max}$ represents the maximum linear acceleration of the UAV. Based on the above analysis, the optional velocity space V_r for the UAV planning process can be obtained, as shown in Eq. (8).

$$V_r = V_m \cap V_{safe} \cap V_F \tag{8}$$

After determining the final optional speed space, the study assumes that the UAV's speed is short and constant, and therefore the impact of acceleration on the UAV can be ignored. In a shorter UAV planning time, if the UAV planning presents a straight line, the UAV trajectory prediction can be obtained based on the UAV motion model, as shown in Eq. (9) [20].

$$(F_x^i - O_x^j)^2 + (F_y^i - O_y^j)^2 = (r_F)^2, \omega_i \neq 0 \tag{9}$$

In Eq. (9), (O_x^j, O_y^j) is the center coordinate of the UAV's motion trajectory. r_F represents the center coordinate radius of the UAV. F_x^i and F_y^i are the horizontal and vertical axis dynamics of the center coordinate point of the UAV. Based on the short and constant speed, the predicted trajectory of the UAV can be obtained, as shown in Eq. (10).

$$\begin{cases} r_F = \left| \dfrac{v_i}{\omega_i} \right| \\ O_x^i = -\dfrac{v_i}{\omega_i} \cdot \sin\theta(t_i) \\ O_y^i = \dfrac{v_i}{\omega_i} \cdot \cos\theta(t_i) \end{cases} \tag{10}$$

In Eq. (10), t_i represents the predicted time. Next, the research needs to evaluate the predicted trajectory of UAVs. If the high score instruction $(v, \omega)_{\max}$ of the UAV is taken as the next sampling control instruction of the UAV, the direction evaluation function is obtained as shown in Eq. (11).

$$F(v,\omega)_{\max} = \sigma\left[\tau \cdot DS(v,\omega) + \gamma \cdot vel(v,\omega) + \varepsilon \cdot HD(v,\omega)\right] \tag{11}$$

In Eq. (11), σ represents normalization processing. γ, ε, and τ are both evaluation weight coefficients. $vel(v,\omega)$, $DS(v,\omega)$, and $HD(v,\omega)$ respectively represent speed, distance, and direction evaluation functions.

B. PP Modeling Based on Multiple UAV Swarms

The previous chapter completed the PP for a single UAV, and the control of UAV swarms has evolved from single-UAV to multi-UAV control, which is subject to more conditional constraints and involves more complex control. For the collision risk and complex planning requirements of multi-UAV cooperative operation, the collision avoidance strategy and collision field division are introduced to solve the potential conflicts between UAVs. Upon analyzing the limitations of forward trajectory prediction and the dynamic window of UAVs, an optimization scheme based on detection radius and information sharing is proposed. A detailed conflict quantification standard is also formulated, encompassing avoidance rules in the front, back, left, right, and upward directions, thereby effectively enhancing the collaborative planning ability and obstacle avoidance performance of the UAV cluster. The multi-machine planning process requires collaborative work to avoid cluster collisions. The difference between single UAV and UAV swarm planning is shown in Fig. 4.

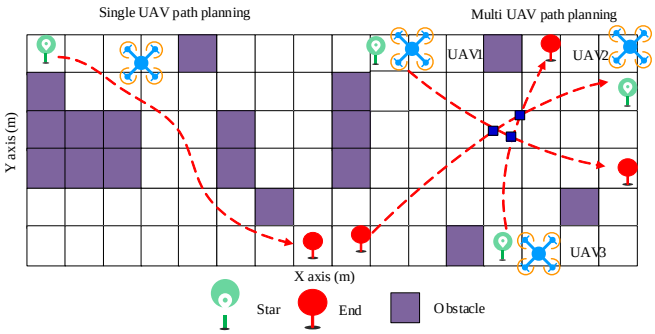

Fig. 4. UAV swarm PP and single UAV PP.

According to the scenario of unmanned cluster planning depicted in Fig. 4, multiple UAVs must navigate to avoid obstacles while not interfering with other UAV operations, all under multiple constraints and within a more complex framework. The single machine planning method obviously does not meet the requirements of collaborative control between UAVs. Therefore, the study introduces UAV conflict avoidance strategies for UAV conflict control. In the conflict analysis of UAVs using the JPS algorithm, it is assumed that the forward trajectory prediction time for all individual machines in the UAV fleet is the same, which is t_i. When the predicted trajectory distance is lower than the safe distance set by the cluster system, it is considered as a flight conflict. If there is an overlap in the predicted trajectories of multiple UAVs, it indicates that the current UAV will have a flight conflict [21]. Considering that the dynamic window in UAV planning only predicts conflicts at forward time t_i, and does not consider the impact on the UAV's own farther distance, the study also introduces collision fields to solve this problem, as shown in Fig. 5.

In Fig. 5, the red inner circle area represents the entire area of UAV safety conflict. UAVs in the red area will not collide, that is, $0 \le d \le r_1 + r_2$. d is the distance between the UAV and the center point, and $r_1 + r_2$ is the radius distance between the two UAVs. When the UAV exceeds the detection range, that is, $d > r_{rule}$, r_{rule} is the detection radius of UAVs 1 and 2, and the green area indicates that the UAV is beyond the recognizable green range, and the UAV is in a low-risk conflict area. If the UAV is within the green range, it is an avoidance area, and there may be potential conflicts within this range. According to the detection of two UAVs moving in the same straight line, the detection radius r_{rule} can be obtained, as shown in Eq. (12).

$$r_{r_{ule}} = r_1 + r_2 + (v_1 + v_2) \cdot t_i \tag{12}$$

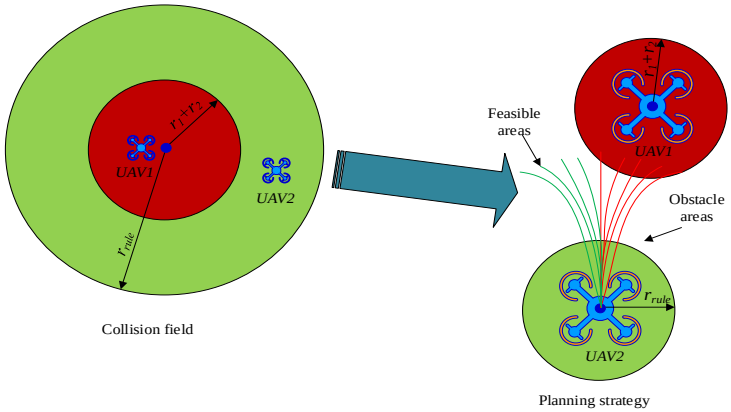

Fig. 5. Division of UAV collision field.

In Eq. (12), v_1 and v_2 are the linear velocities of UAVs 1 and 2, respectively. To ensure that UAVs can detect objects and escape in a timely manner before conflicts occur, research needs to use the maximum value of r_{rule} as the detection radius for all UAVs in the fleet. In addition, the inability to use velocity space to predict dynamic obstacle trajectories during UAV flight can lead to local optimal planning problems in UAV planning, as shown in Fig. 6 [22].

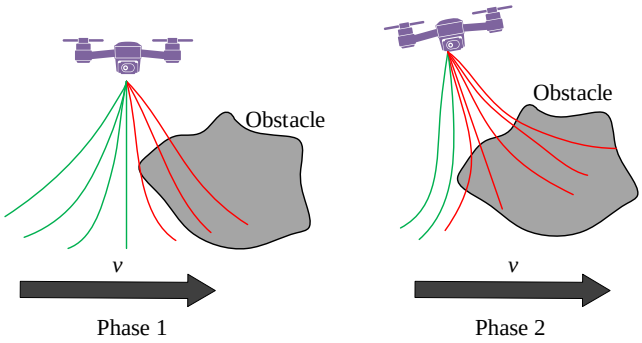

Fig. 6. Dynamic obstacle UAV planning scenario.

From stage 1 in Fig. 6, the UAV will select a green safe trajectory for planning to avoid dynamic obstacles ahead. However, in the second stage, if the obstacle movement speed is equal to or greater than the planned speed of the UAV, it will result in its inability to effectively yield to the obstacle [23]. At this moment, the UAV can only decelerate and evade, awaiting the lifting of the speed space limit. The UAV can maintain its original planned route or turn right to take a detour. To avoid such problems, the research adds a cluster information exchange mechanism, which means that different UAV motion states are shared with each other, providing an effective selectable speed space for the next UAV in advance [24]. Meanwhile, flight planning is carried out according to conflict avoidance rules, including conflicts in the front, rear, left, and right directions. The quantification standard for forward conflicts is shown in Eq. (13).

$$|\ell_{cg}| < \frac{\pi}{36} \tag{13}$$

In Eq. (13), ℓ_{cg} represents the azimuth angle of unmanned aerial vehicl UAV_c e relative to the current UAV UAV_g. If UAV_c is located in front of UAV_g, there will be two situations where the UAV flies in the same or opposite direction. Regardless of which scenario, UAV_c remains in its original state, while UAV_g uses left or right planning to avoid obstacles [25]. The quantification standard for the right side conflict is shown in Eq. (14).

$$-\frac{5}{8}\pi \le \ell_{cg} < -\frac{\pi}{36} \tag{14}$$

In the right side conflict, UAV_c is located to the right of UAV_g and has the highest flight priority. Currently, UAV UAV_g needs to slow down or turn left to avoid. The left side conflict quantification standard is shown in Eq. (15) [26].

$$\frac{\pi}{36} \le \ell_{cg} < \frac{5}{8}\pi \tag{15}$$

In the left side conflict, UAV_c is located to the left of UAV_g, which has the highest flight priority. The conflicting UAV UAV_c needs to slow down or turn right to avoid. The quantification standard for post burst is shown in Eq. (16).

$$|\ell_{cg}| \ge \frac{5}{8}\pi \tag{16}$$

In the rear conflict, UAV_c is located behind UAV_g, and UAV_g also has the highest flight priority. It maintains its original flight state unchanged, while aircraft UAV_c takes the initiative to avoid to the left or right.

III. RESULTS

A. Single Machine PP Experiment

Next, the research conducted experiments on the proposed UAV PP technology, setting the UAV flight experiment scene to various specifications of grid maps, including 30m×30m, 38m×38m, etc. Meanwhile, in the implementation of UAV flight PP, experiments were conducted by dividing static and dynamic obstacle scenarios. The details of the experimental hardware setup are presented in Table I.

In the experimental analysis, common UAV planning algorithms A* and JPS were introduced as tests to confirm the validity of different techniques in regard to control error, planning length, number of expansion nodes, and planning duration. The study selected a 38m×38m grid map environment for UAV flight control experiments, and the test outcomes are in Fig. 7.

TABLE I DETAILS ABOUT THE EXPERIMENTAL SETUP

Experimental environment	Model
Experimental System Platform	Windows 11
Experimental processor	AMD 3800X
Graphics card	NVIDIA RTX3070
Computer operating memory	32 RAM
Hard disk capacity	1T
Simulation experimental platform	MATLAB

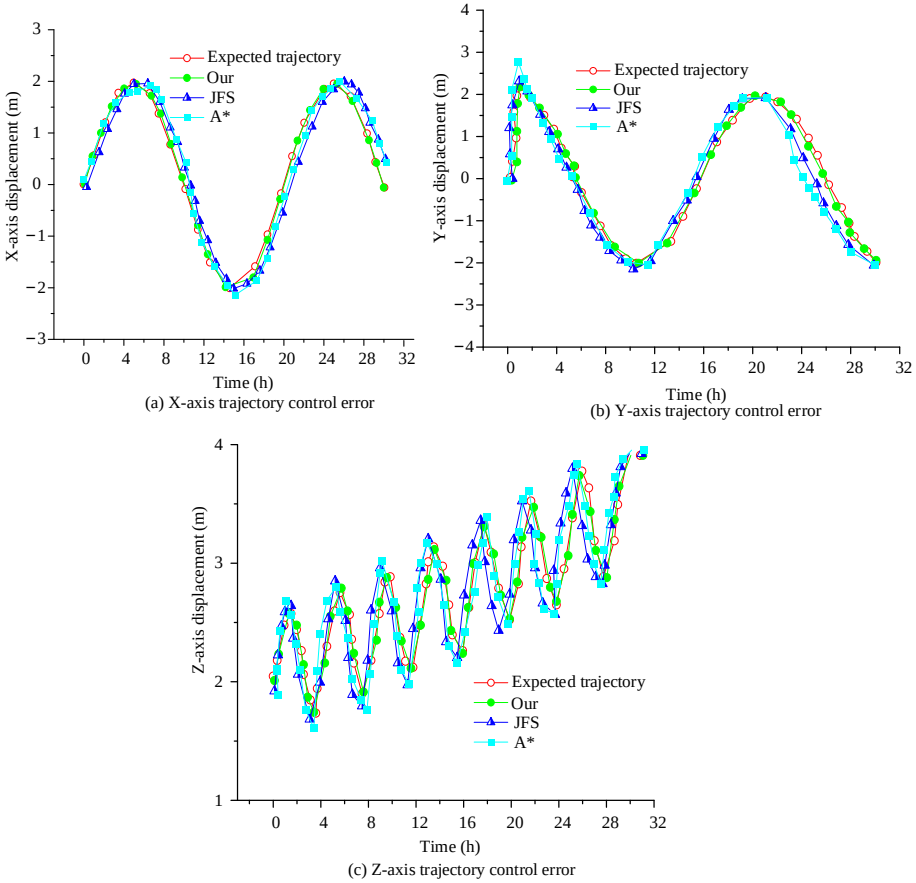

Fig. 7. Experimental analysis of flight control error for a single UAV.

Fig. 7(a) shows the control error of the UAV in the X-axis direction. According to the curve changes, at the 32nd hour of the UAV flight, the expected trajectory in the X-axis was -0.020m, the research model was -0.0019m, while JPS and A* were 0.4984m and 0.4935m, respectively. Overall, the control error of the research model was lower, with an improvement of 7.25% and 9.28% in accuracy compared to the JPS and A* control errors. Fig. 7(b) shows the analysis outcomes of the control error of the UAV in the Y-axis direction. At the 2nd and 26th hours of flight, A* and JPS had significant deviations in control accuracy and predicted trajectory in the Y-axis direction. In the second hour, A* planning was unable to effectively screen out effective planning nodes, resulting in them exceeding the expected trajectory by 0.56m. Meanwhile, JPS also exceeded the expected trajectory by 0.25m. Only the research model controlled the error at 0.12m, resulting in better overall control accuracy. Fig. 7(c) shows the control error of the UAV in the Y-axis direction. Only the research model could follow the expected trajectory well, with an overall deviation controlled within the range of 0.05m. However, A* flight planning was the worst, such as in UAV turning scenarios at the 4th and 8th hours, where A*'s following control was significantly insufficient. JPS also faced similar problems. Next, a 30m×30m grid map was selected for static scene planning testing, and the test results are shown in Fig. 8.

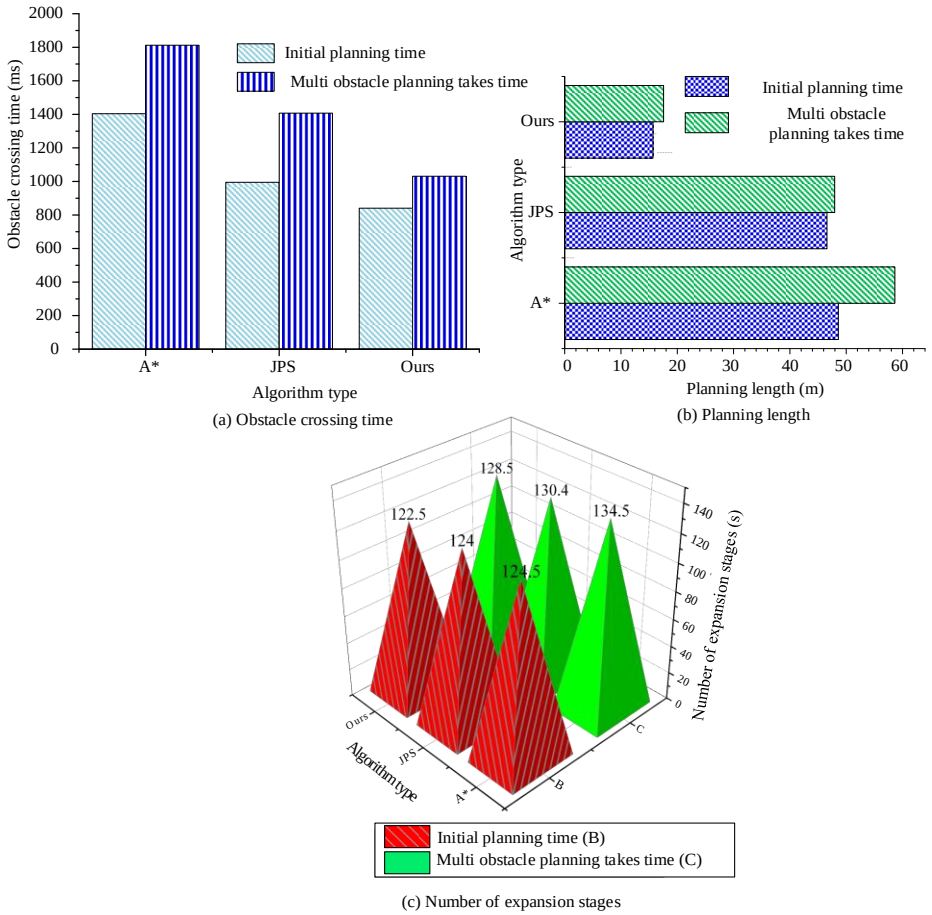

Fig. 8. Comparison of comprehensive effects of static PP for UAVs.

Fig. 8(a) shows the comparison of obstacle crossing time. In the initial planning, A* took 1401ms, JPS was 1002ms, and the research model was 885ms. However, in the multi-obstacle planning, the overall time of the research model was the shortest, only 1002ms. The comparison of PP length is shown in Fig. 8(b). The research model had the lowest planning length in both the initial planning and multi-obstacle planning, which were 15.25m and 17.85m, respectively, while JPS and A* had planning lengths of 49.85m and 58.054m, respectively. Fig. 8(c) shows the comparison of the number of extended nodes in PP. The research model had a significantly lower number of extended nodes in PP, with 122.5 nodes in the research model, 124.5 nodes in A*, and 124.0 nodes in JPS. In multi-obstacle planning, the research model had 128.5 extended nodes, which was significantly lower than the other two techniques. This indicated that it had lower resource utilization and better planning efficiency in planning. Finally, a 38m×38m grid map was selected for PP testing, as shown in Fig. 9.

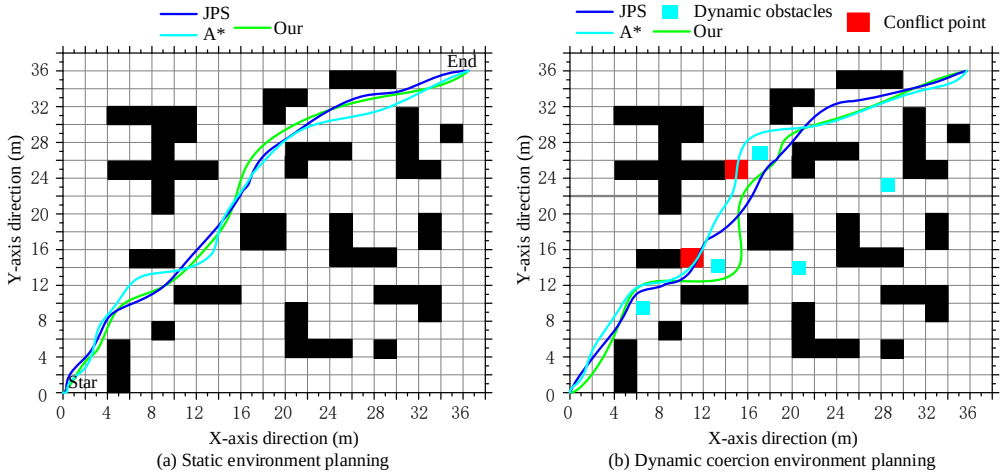

Fig. 9. Static and dynamic obstacle PP test.

Fig. 9(a) shows the results of static environmental PP, where the UAV crossed obstacles from the starting point to the endpoint. The final planned length of the research model was 59.2m, while JPS was 61.2m and A* was 63.2m. Fig. 9(b) shows the results of dynamic obstacle planning scenarios. The blue area represents dynamic obstacles, and the red area represents conflict points. According to the results, A* experienced two conflicts during the planning process, which led to an increase in both its planning length and time. Meanwhile, JPS also encountered conflicts with the first dynamic obstacle, necessitating avoidance maneuvers. The final planned lengths of JPS and A* were 68.2m and 70.2m, respectively. However, the research model effectively predicted the trajectory of dynamic obstacles and avoids waiting, with the shortest planned distance being 63.28m.

B. UAV Swarm PP Experiment

Next, the research continued to test the PP of multi-person airport scenery, with consistent experimental environments. The research compared DWA-JPS with DWA-JPS that combined conflict avoidance strategies (Ours). Firstly, the study selected local planning quantities for UAV conflict planning for testing, as shown in Fig. 10.

Fig. 10(a) and 10(b) show the conflict planning results of DWA-JPS and Ours, respectively. In the DWA-JPS planning, both forward-moving UAVs opted to evade obstacles by veering left and right, which led to both UAVs altering their intended destinations and becoming trapped in local optima, rendering it impossible to re-plan their predestined trajectories. In Ours conflict planning, the two UAVs adopted a conflict avoidance strategy, successfully separated and detoured back to their original trajectory. Next, a 30m×30m grid map was selected for multi-UAV planning testing, as shown in Fig. 11.

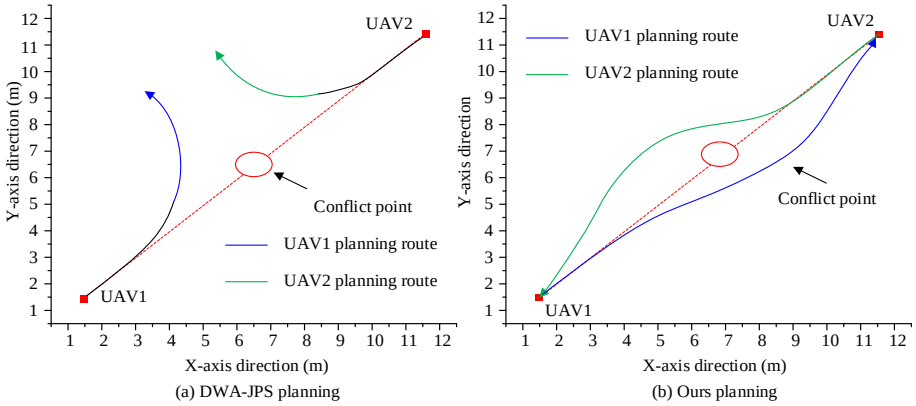

Fig. 10. Local conflict planning test.

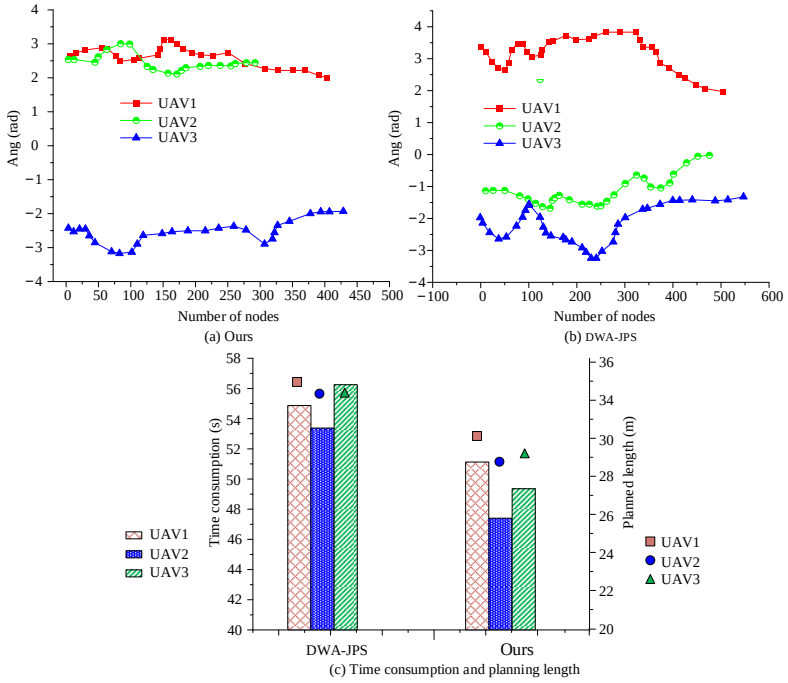

Fig. 11. Multi-UAV planning test.

Fig. 11(a) and 11(b) show the PP of Ours and DWA-JPS, respectively. There were significant differences in the planning angles between the two types of UAVs, but the number of expansion nodes in Ours planning was significantly lower. For example, in Ours planning, UAV 2 had 324 expansion nodes, while DWA-JPS had 501. Fig. 11(c) shows the results of time consumption and planning length. According to the results, the average time consumption in DWA-JPS planning was 55.2s, while Ours was 49.8s, indicating that the research model had a shorter planning time. In the comparison of planning lengths, the average planning length of Ours was 29.3m, while that of DWA-JPS was 55.3m. The planning technology proposed in the study performed better overall. Finally, the study selected 19m×19m and 29m×29m grid maps for comparison of planning effects, as shown in Fig. 12.

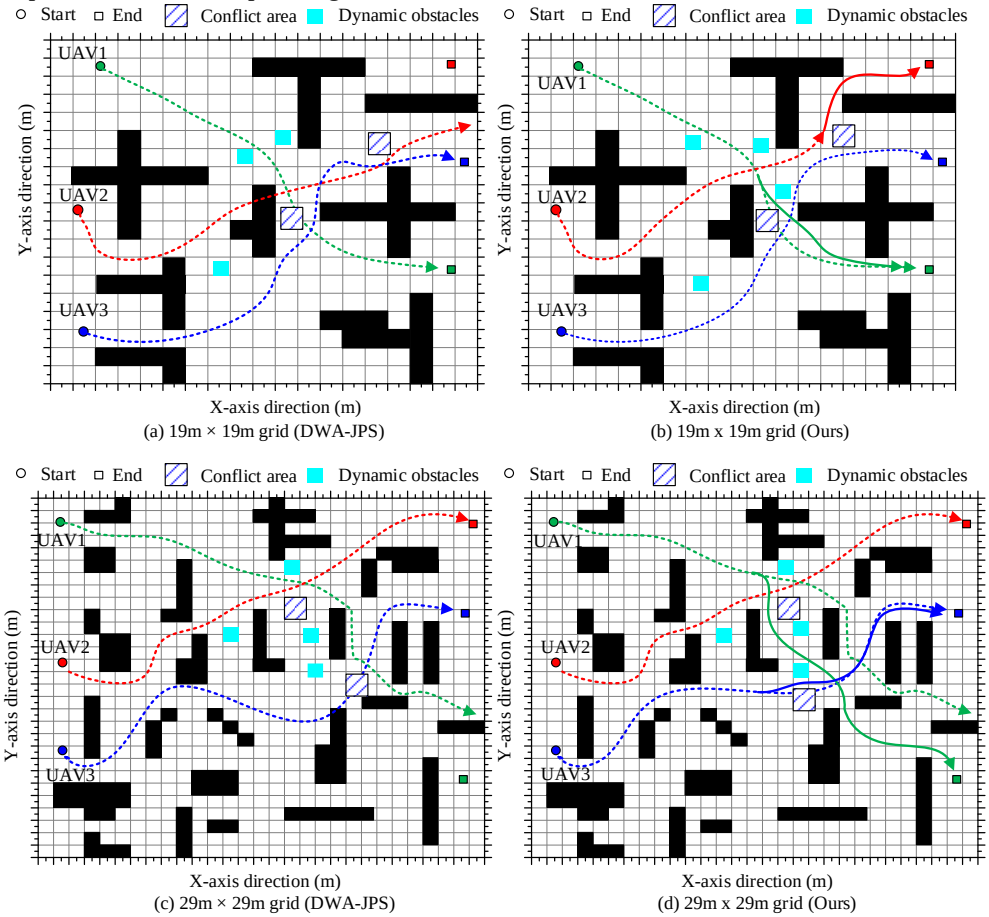

Fig. 12. PP test for 19m×19m and 29m×29m grid maps.

Fig. 12(a) and 12(b) show the planning results of DWA-JPS and Ours on a 19m×19m grid map. In the DWA-JPS PP, there was a clear conflict at the intersection of three UAVs, causing UAV 2 to avoid the right and fall into local convergence, unable to reach the target location smoothly. Meanwhile, the collision between UAV 1 and UAV 3 resulted in waiting and avoidance, leading to an extension of the planned distance. In Ours planning, the conflict avoidance strategy adopted by the research model in the conflict area was studied, and the route planning was re-conducted. There was no local convergence in the UAV 2 area, and the avoidance strategy also allowed the remaining UAVs to bypass the conflict in a shorter time and return to the predetermined planned trajectory. Fig. 12(c) and 12(d) show the planning results of DWA-JPS and Ours on a 29m×29m grid map. In DWA-JPS planning, UAV 1 still chose to avoid to the left at the conflict point, causing it to fall into local convergence and unable to return to the designated planned trajectory. The long waiting time of UAV 3 at the conflict point also affected the planning effectiveness. Ours adopted an avoidance strategy at the conflict point, predicting the conflict ahead and avoiding the wait for conflicts, thus preventing the problem of local convergence in planning, with the best overall performance. Next, three UAV road planning scenarios (10m×10m, 19m×19m, 29m×29m and 38m×38m) were selected for experiments to compare the average planning time of UAV groups with different technologies. The results are shown in Table II.

Table II shows the time-consuming comparison of road scenario planning for multi-UAV planning. Four planning scenarios were selected for comparison. Overall, Ours fleet planning was the best. For example, the average planning time of UAV 1 under four roads was 34.3s, while the average planning time of DWA-JPS was 39.0s. Especially in the more complex 38m×38m road planning, the average planning time of UAV 1, UAV 2 and UAV 3 in Ours was 34.3s, 34.2s and 34.0s, which was significantly better than 39.0s, 39.5s and 39.6s of DWA-JPS.

TABLE II COMPARISON OF AVERAGE PLANNING TIME OF UAV GROUP

Planning road scenarios	DWA-JPS (s)			Ours (s)		
	UAV1	UAV2	UAV3	UAV1	UAV2	UAV3
10m×10m	12.5	11.6	12.8	9.3	9.7	9.5
19m×19m	21.6	22.5	23.5	17.6	17.8	16.8
29m×29m	52.3	53.5	52.8	47.5	45.5	46.8
38m×38m	69.5	70.5	69.2	62.8	63.8	62.8
Average comprehensive time	39.0	39.5	39.6	34.3	34.2	34.0

IV. DISCUSSION AND CONCLUSION

With the swift advancement of UAV technology, multi-UAV collaborative PP has emerged as a study hotspot. To improve the effectiveness of multi-UAV PP, a multi-UAV PP technique based on an improved JPS algorithm was proposed and relevant experiments were conducted.

In single UAV PP, taking the 38m×38m grid map environment as an example, compared with A* and JPS algorithms, the proposed model improved the accuracy of X-axis control error by 7.25% and 9.28%, and had lower Y-axis control error. In static scene planning tests, the planning time was the shortest, and the PP length and number of extended nodes were better than the other two techniques. In dynamic obstacle planning scenarios, the proposed model could effectively predict the trajectory of dynamic obstacles, avoid waiting, and plan the shortest distance. The reason why the research technology was superior to traditional JPS and A* is that the introduction of geometric collision detection strategy improved the path search range. In addition, the introduction of DWA to predict the conflict range significantly improved the technical adaptability.

In terms of PP for multiple UAV swarms, the research was based on distributed control clusters and introduced UAV conflict avoidance strategies for planning. By setting collision fields and conflict avoidance rules, the problem of mutual collision among UAV swarms during collaborative operations was effectively solved. The experiment compared DWA-JPS with Ours, and the results showed that in the local conflict planning test, Ours could smoothly separate and return to its original trajectory, while DWA-JPS fell into local optima. In the multi-UAV planning test of 30m×30m grid map, Ours planning showed significantly lower number of expansion nodes, shorter planning time, and better average planning length. In the comparison of planning effects on grid maps of different sizes, Ours adopted a conflict avoidance strategy in conflict areas, avoiding local convergence and planning getting stuck in local optima, resulting in the best overall performance.

To sum up, the research technology performed well in the field of UAV planning, including: In the PP of single UAV, it significantly reduced the control error, shortened the length and time of PP, reduced the number of expansion nodes, and improved the effect of dynamic planning; In the multi UAV PP, the conflict between UAVs was effectively avoided, the local optimal problem was solved, the planning efficiency was improved, and the good cooperative operation ability was displayed. However, there are also shortcomings in the research technology, as it has not taken into account the influence of more dynamic objects in the air environment. In addition, more motion characteristics of UAVs have not been taken into account. In the future, it is necessary to fully consider the above issues and improve technological adaptability.

REFERENCES

[1] Lee H, Cho S, Jung H. Real-time collision-free landing path planning for drone deliveries in urban environments. ETRI Journal, 2023, 45(5): 746-757.

[2] Shen K, Shivgan R, Medina J, Dong Z. Multidepot drone path planning with collision avoidance. IEEE Internet of Things Journal, 2022, 9(17): 16297-16307.

[3] Meng S, Gao Z, Zhou Y, He B. Real-time automatic crack detection method based on drone. Computer-Aided Civil and Infrastructure Engineering, 2023, 38(7): 849-872.

[4] Bui S T, Luu Q K, Nguyen D Q, Le NDM. Tombo propeller: bioinspired deformable structure toward collision-accommodated control for drones. IEEE Transactions on Robotics, 2022, 39(1): 521-538.

[5] Fahimi H, Mirtajadini S H, Shahbazi M. A vision-based guidance algorithm for entering buildings through windows for delivery drones. IEEE Aerospace and Electronic Systems Magazine, 2022, 37(7): 32-43.

[6] Saeed R A, Omri M, Abdel-Khalek S, Ali ES. Optimal path planning for drones based on swarm intelligence algorithm. Neural Computing and Applications, 2022, 34(12): 10133-10155.

[7] Puente-Castro A, Rivero D, Pazos A, Blanco E F. A review of artificial intelligence applied to path planning in UAV swarms. Neural Computing and Applications, 2022, 34(1): 153-170.

[8] Dhuheir M A, Baccour E, Erbad A, Erbad A. Deep reinforcement learning for trajectory path planning and distributed inference in resource-constrained UAV swarms. IEEE Internet of Things Journal, 2022, 10(9): 8185-8201.

[9] Sharma A, Shoval S, Sharma A, Pandey J K. Path planning for multiple targets interception by the swarm of UAVs based on swarm intelligence algorithms: A review. IETE Technical Review, 2022, 39(3): 675-697.

[10] Yu Z, Si Z, Li X, Wang D, Song H. A novel hybrid particle swarm optimization algorithm for path planning of UAVs. IEEE Internet of Things Journal, 2022, 9(22): 22547-22558.

[11] Li J, Xiong Y, She J. UAV path planning for target coverage task in dynamic environment. IEEE Internet of Things Journal, 2023, 10(20): 17734-17745.

[12] Wan Y, Zhong Y, Ma A, Zhang L. An accurate UAV 3-D path planning method for disaster emergency response based on an improved multiobjective swarm intelligence algorithm. IEEE Transactions on Cybernetics, 2022, 53(4): 2658-2671.

[13] Roque-Claros R E, Flores-Llanos D P, Maquera-Humpiri A R, et al. UAV Path Planning Model Leveraging Machine Learning and Swarm Intelligence for Smart Agriculture. Scalable Computing: Practice and Experience, 2024, 25(5): 3752-3765.

[14] Luo J, Liang Q, Li H. UAV penetration mission path planning based on improved holonic particle swarm optimization. Journal of Systems Engineering and Electronics, 2023, 34(1): 197-213.

[15] Shahid S, Zhen Z, Javaid U. Multi-UAV path planning using DMGWO ensuring 4D collision avoidance and simultaneous arrival. Aircraft Engineering and Aerospace Technology, 2024, 96(9): 1117-1127.

[16] Lu L, Fasano G, Carrio A. A comprehensive survey on non-cooperative collision avoidance for micro aerial vehicles: Sensing and obstacle detection. Journal of Field Robotics, 2023, 40(6): 1697-1720.

[17] Suanpang P, Jamjuntr P. Optimizing autonomous UAV navigation with d algorithm for sustainable development. Sustainability, 2024, 16(17): 7867-7875.

[18] Junkai Y, Xueying S, Hongyue C. Hybrid particle swarm optimisation approach for 3D path planning of UAV. International Journal of Bio-Inspired Computation, 2023, 22(4): 227-236.

[19] Zheng J, Ding M, Sun L, Liu H. Distributed stochastic algorithm based on enhanced genetic algorithm for path planning of multi-UAV cooperative area search. IEEE Transactions on Intelligent Transportation Systems, 2023, 24(8): 8290-8303.

[20] Venkatasivarambabu P, Agrawal R. Enhancing UAV navigation with dynamic programming and hybrid probabilistic route mapping: an improved dynamic window approach. International Journal of Information Technology, 2024, 16(2): 1023-1032.

[21] Bulut F, Bektaş M, Yavuz A. Efficient path planning of drone swarms over clustered human crowds in social events. International Journal of Intelligent Unmanned Systems, 2024, 12(1): 133-153.

[22] Beishenalieva A, Yoo S J. Multiobjective 3-D UAV movement planning in wireless sensor networks using bioinspired swarm intelligence. IEEE Internet of Things Journal, 2022, 10(9): 8096-8110.

[23] Tian S, Li Y, Zhang X, Zheng L, Cheng L, She W. Fast UAV path planning in urban environments based on three-step experience buffer sampling DDPG. Digital Communications and Networks, 2024, 10(4): 813-826.

[24] Xiangyu W, Yanping Y, Dong W, Zhang Z. Mission-oriented cooperative 3D path planning for modular solar-powered aircraft with energy optimization. Chinese Journal of Aeronautics, 2022, 35(1): 98-109.

[25] De Guzman C J P, Sorilla J S, Chua A Y. Ultra-Wideband Implementation of Object Detection Through Multi-UAV Navigation with Particle Swarm Optimization. International Journal of Technology, 2024, 15(4): 1026-1036.

[26] Alotaibi A, Chatwin C, Birch P. Evaluating Global Navigation Satellite System (GNSS) Constellation Performance for Unmanned Aerial Vehicle (UAV) Navigation Precision. Journal of Computer and Communications, 2024, 12(9): 39-62.